ACS APPLIED MATERIALS & INTERFACES

Research Article

www.acsami.org

Building Nanoporous Metal–Organic Frameworks "Armor" on Fibers for High-Performance Composite Materials

Xiaobin Yang,[†] Xu Jiang,[†] Yudong Huang,[†] Zhanhu Guo,[*,§] and Lu Shao[*,†]

[†]MIIT Key Laboratory of Critical Materials Technology for New Energy Conversion and Storage, State Key Laboratory of Urban Water Resource and Environment, School of Chemistry and Chemical Engineering, Harbin Institute of Technology, Harbin, China

[§]Integrated Composites Laboratory (ICL), Department of Chemical & Biomolecualr Engineering, University of Tennessee, Knoxville, Tennessee 37996, United States

Supporting Information

ABSTRACT: The nanoporous metal–organic frameworks (MOFs) "armor" is in situ intergrown onto the surfaces of carbon fibers (CFs) by nitric acid oxidization to supply nucleation sites and serves as a novel interfacial linker between the fiber and polymer matrix and a smart cushion to release interior and exterior applied forces. Simultaneous enhancements of the interfacial and interlaminar shear strength as well as the tensile strength of CFs were achieved. With the aid of an ultrasonic "cleaning" process, the optimized surface energy and tensile strength of CFs with a MOF "armor" are 83.79 mN m^{-1} and 5.09 GPa, for an increase of 102% and 11.6%, respectively. Our work finds that the template-induced nucleation of 3D MOF onto 1D fibers is a general and promising approach toward advanced composite materials for diverse applications to meet scientific and technical demands.

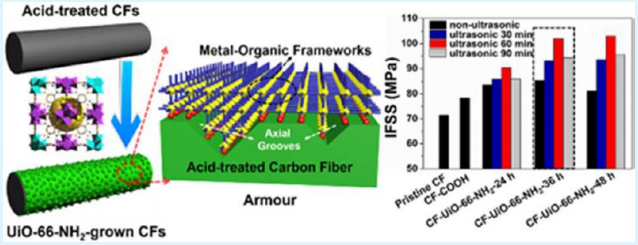

KEYWORDS: *metal–organic frameworks, 1D fibers, surface modification, strength, composite materials*

1. INTRODUCTION

Various fibers have been used to prepare composite materials for diverse applications, such as aerospace, electronics, civil engineering, and leisure sports, which produce billions of dollars of revenue annually. Therefore, high-performance fiber-reinforced composites are highly desirable for economic and practical considerations.[1−5] Theoretically, a favorable interphase between the fiber and polymer matrix is essential to the performance of fiber-reinforced composites. The interphase strengthens the fiber–matrix compatibility and load transfer efficiency to meet the demands of scientific and technical evolution.[6−10] However, limitations on the physicochemical structure and surface properties of 1D fibers, such as the typical smoothness, chemical amphiphobic, and inertness features, lead to nonideal interfacial combination, deteriorating the properties of the resultant fiber-reinforced composites.[11−13] Surface modifications of 1D fibers have been proposed as the most convenient way to address this challenge. Current surface modifications of 1D fibers include chemical oxidation, γ-ray irradiation, chemical grafting, and coating, which can increase the surface roughness for mechanical interlocking and the surface energy for wettability and chemical bonding activity.[14−23] However, these treatments may cause damages to the inherent strength of the fibers due to high energy or catalyst processing and can result in excessive steps, reduction in the fiber volume fraction in the composites, and poor wettability between the fibers and matrix due to hydrophobic nanomaterial grafting.[24−30] Therefore, an effective strategy to simultaneously enhance the roughness, surface energy, and overall mechanical properties of 1D fibers is needed to achieve "superior" fiber-reinforced composites.

Metal–organic frameworks (MOFs) are an emerging class of nanoporous coordination materials that have garnered significant attention due to their tunable nanoscale pore structures, large specific surface areas, skeletal structure diversity, unsaturated metal sites, and exchangeable ligands.[31−35] The unique features of nanoporous 3D MOF can overcome the demerits of 1D fibers for advanced composite materials. Recently, a zirconium-based UiO-66 MOF with the highest coordination number of 12, relatively high BET specific surface area (over 1000 m^2 g^{-1}), excellent thermal stability (considering following participation in CF-reinforced composite curing procedure), solvent resistance, and outstanding shear strength (as high as 13.75 GPa) has been investigated for gas separation, catalysis, and drug delivery applications.[36−41] Considering the inherent organic–inorganic hybrid feature of MOFs, and the reaction mechanism of typical polymer matrixes in fiber-reinforced composites, amino-functionalized UiO-66-NH_2 is an interesting material for tuning the fiber surface properties to enhance the performance of fiber-reinforced composites.[11,21,42−47] Meanwhile, the polar functional moieties in UiO-66-NH_2 scaffolds are beneficial to the resultant enhanced surface energy and wettability. Also, they were confirmed to be capable of reacting with polymers to fabricate

Received: November 24, 2016
Accepted: January 19, 2017
Published: January 19, 2017

DOI: 10.1021/acsami.6b15098
ACS Appl. Mater. Interfaces 2017, 9, 5590−5599

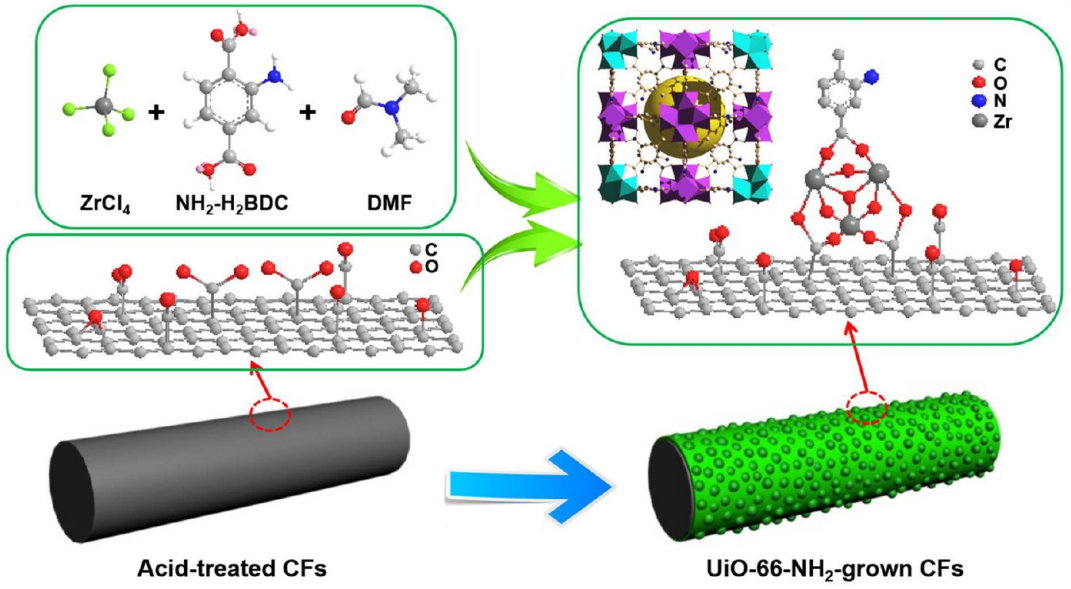

Figure 1. Schematic illustration of the possible UiO-66-NH_2 crystallization mechanism on CFs. The topological crystalline structure of MOF UiO-66-NH_2 after eliminating H atoms is inserted in the right rounded rectangle. The dummy yellow sphere corresponds to the void space located centrally to the unit cell and an octahedral cage consisting of six purple polyhedrons simultaneously (C, gray; O, red; N, blue; Zr, dark). The O active sites at the fringe are for extended framework connectivity.

mixed matrix membrane.[48] Moreover, amino groups in its scaffolds could be involved in the curing reaction between epoxy resin and curing agent. Therefore, we believe that the acidized surface of 1D fibers is an ideal platform for the in situ growth of MOF because the functional groups, such as carboxylate groups, on the acidized fiber surface can act as nucleation sites for the crystallization of MOF. The 3D MOF grown onto 1D fibers as a new organic−inorganic hybrid "armor" can generate additional roughness, improve the surface energy, enhance the comprehensive mechanical properties of fibers, increase the contact area between the fibers and organic matrix, and release the applied force in composites, resulting in high-performance composites by simple surface/interface manipulation.

As a proof of concept, we generate carboxyl groups on the surface of 1D carbon fibers (CFs) by nitric acid oxidization to supply nucleation sites for the in situ construction of a 3D nanoporous MOF "armor" on the fibers. Using this facile strategy, we find that nanoporous MOF can be utilized as a favorable platform to improve the surface/interface properties of fibers for high-performance fiber-reinforced composites. Figure 1 displays a schematic illustration of the fabrication of (UiO-66-NH_2 type) MOF-coated CFs, and the inset shows the UiO-66-NH_2 topological crystalline structure after eliminating H atoms. UiO-66-NH_2 coating can be easily formed on the carboxyl-activated surface of CFs at 80 °C (a mild condition) from metal salt ($ZrCl_4$) and organic ligand (2-amino-terephthalic acid: NH_2-H_2BDC) in *N*,*N*-dimethylformamide (DMF) solution. During this process, two key points should be noted: (1) the "growing" time of MOF affects the quantity of MOF "armor" on the 1D fibers, and the optimal crystallization time will be investigated and determined in this study; (2) even though the dense MOF "armor" has been successfully formed on the surface of the fibers, some nanocrystals, formed as "impurities" in the reaction system, will physicochemically absorb on the outside of the MOF "armor", just like dust on a cloth, and cannot be removed by simple washing. Although these nanocrystals are beneficial to the tensile strength of the fibers, the performance of the fiber-reinforced composites is greatly deteriorated due to the "weak" points induced by these nanocrystals on the fiber/resin interface; the "vulnerable" bonds between the MOF "armor" and the attached nanocrystals provide a lubricant effect with respect to the areas covered by the "firm" bonds between MOF and the fibers. To overcome this obstacle, ultrasonic cleaning is adopted to remove the attached nanocrystals to obtain advanced composite materials.

2. EXPERIMENTAL SECTION

2.1. Materials. Carbon fiber (T700-12000-50C) (diameter: 7 μm; density: 1.8 g cm^{-3}) was acquired from Toray Industries Inc. and was subjected to Soxhlet extraction with acetone at 70 °C for 48 h to eliminate the surface sizing and contamination prior to use. Zirconium(IV) chloride ($ZrCl_4$, ≥99.9%) was purchased from Aladdin (China). 2-Aminoterephthalic acid (NH_2-H_2BDC, 99%) was obtained from Sigma-Aldrich (USA). *N*,*N*-Dimethylformamide (DMF), fuming nitric acid (HNO_3), acetone, and methanol were obtained from Tianjin Kermel Chemical Reagent Co., Ltd. (China). E51 epoxy resin matrix (viscosity 2500 mPa s at 40 °C and epoxide value 0.48−0.54 equiv/100 g) was provided by Bluestar Wuxi Petrochemical Co., Ltd. (Jiangsu, China). H-256, used as a curing agent, was provided by Jiangyin Wayfar Synthetic Material Co., Ltd. (Jiangsu, China). Ultrapure water (18.0 MΩ·cm) was produced using a Sartorius AG arium system and was used in all experiments. All chemical reagents and solvents were used as received.

2.2. Fabrication of UiO-66-NH_2-Functionalized CFs. Nitric acid-treated CFs (denoted as CF-COOH) were prepared by immersing a certain amount of extracted CFs in a flask with HNO_3 at 80 °C for 4 h, rinsing with ultrapure water several times until reaching a neutral pH, and drying under vacuum at 70 °C overnight. A typical precursor solution of UiO-66-NH_2 was prepared by mixing two DMF solutions (50 mL) of $ZrCl_4$ (0.83 g) and NH_2-H_2BDC (0.89 g) at room temperature under stirring. Then, the mixture was transferred and sealed in a single-necked flask, with a glass frame rounded by CF-COOH. The flask was heated to 80 °C and held for 24, 36, or 48 h. After undisturbed incubation and thoroughly rinsing with DMF, methanol, and deionized water, the obtained UiO-66-NH_2-functionalized CFs were ultrasonically treated in water. Subsequently, CFs

DOI: 10.1021/acsami.6b15098
ACS Appl. Mater. Interfaces 2017, 9, 5590−5599

were dried under vacuum at 70 °C overnight. A systematic investigation of the ultrasonic process for 30, 60, or 90 min was performed. After cooling, the homogeneous nucleated yellow powder in the flask was centrifuged (8000 rpm), rinsed with DMF and methanol, and dried under vacuum at 70 °C overnight.

2.3. Physicochemical Characterizations of Various CFs. FTIR measurements were performed using a Spectrum One instrument (PerkinElmer, USA). XPS measurements were conducted on an AXIS ULTRA DLD spectrometer (SHIMADZU, Japan). The morphologies of the aforementioned CFs were observed by SEM (Hitachi S-4500, Japan), and elemental composition analysis was performed by EDX. The XRD spectra were obtained by a RINT D/MAX-2500/PC XRD instrument (Rigaku, Japan) using Cu Kα_1 (λ = 0.154 nm) radiation. All samples were analyzed by a 2θ scan from 5° to 80° with a 0.02° step. The weight loss of UiO-66-NH_2 and CFs was recorded by a thermal gravimetric analyzer (Q500, TA Instruments, USA) from room temperature to 1000 °C at a heating rate of 10 °C min^{-1} under a nitrogen atmosphere. Dynamic contact angle tests were performed to calculate the surface energy of the CFs by immersing four single fibers into two different test liquids using a dynamic contact angle meter and tensiometer (DCAT21, Data Physics Instruments, Germany). The dynamic contact angles of fibers could be calculated using the dynamic contact angle software from the relationship between the fiber immersing depth and the recorded weight values by controlling the movement of the lifting platform. To better demonstrate this test procedure, the optical photos of this instrument and operational schematic diagram are shown as Figure S1. Deionized water (γ_l^d = 21.8 mN m^{-1}, γ_l^p = 51 mN m^{-1}) and ethylene glycol (γ_l^d = 29.0 mN m^{-1}, γ_l^p = 19.0 mN m^{-1}) were used as test liquids. Each sample was measured eight times, and the valid results were averaged to determine the CF surface energy. Through collecting average 30 data per sample from the cross-sectional SEM images of the fiber filaments, we calculated out the statistical thicknesses of MOF layers of various CFs.

2.4. Mechanical Property Measurements of the CFs and Composites. Interfacial evaluation equipment (FA620, Japan) was used to measure interfacial shear strength (IFSS) by pulling off the cured epoxy resin droplets from a filament with both ends fixed. The testable resin beads were fabricated by dotting the E-51/H-256 (w/w, 100/32) mixture with a steel pin, curing at 90 °C for 2 h, 120 °C for 2 h, 150 °C for 3 h, and then annealing at room temperature. At least 50 specimens were collected and averaged per sample. The single-filament tensile measurement was performed to determine the tensile strength (TS) of the CFs on an electronic mechanical universal material testing machine (Instron 5500R, USA) according to ASTM D3379-75. Using a 20 mm gauge length and a 10 mm/min loading speed, at least 80 specimens were tested per sample, and the results were further analyzed using Weibull statistical methods. We evaluated the interlaminar shear strength (ILSS) of the fiber composites using a universal testing machine (5569, Instron, USA) according to ASTM D2344. For the specimen fabrication, the resulting resin volume content was 35 ± 1%, curing was performed at 90 °C for 2 h, the pressure was increased to 5 MPa after the gel formed at this stage, curing continued at 120 °C for 2 h and 150 °C for 4 h under 10 MPa, and the samples were cooled to room temperature while maintaining the pressure. The testing sample dimensions were 25 mm × 6.5 mm × 2 mm. Five specimens were recorded and averaged per sample.

3. RESULTS AND DISCUSSION

3.1. Physicochemical Characterization of Various CFs. Figure 2 presents the FTIR spectra of the bare CF, CF-COOH, and UiO-66-NH_2 grown CFs as well as the resultant UiO-66-NH_2 powder collected from the suspension for chemical groups' analysis. For the untreated fibers, there are no discernible and typical peaks observed from the spectra. As for CF-COOH, under the strong oxidation effect brought from nitric acid to the superficial chemical structures of pristine CFs, several characteristic peaks emerged. The location centered at 3400 cm^{-1} corresponds to the −OH stretching vibration, and

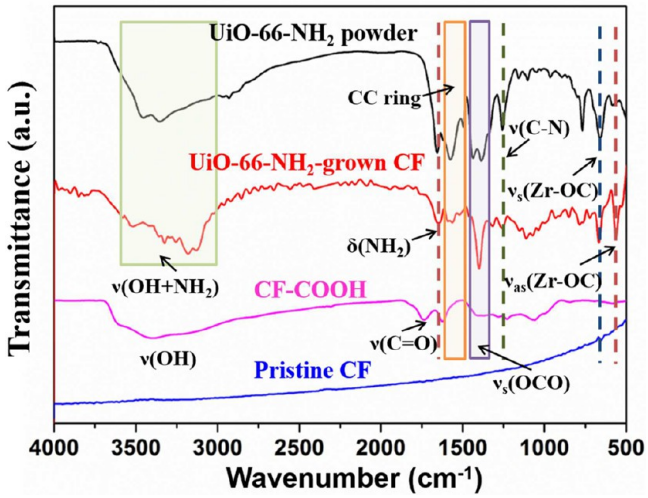

Figure 2. FTIR spectra of the pristine CF, CF-COOH, UiO-66-NH_2-grown CF, and UiO-66-NH_2 powder.

1730 cm^{-1} is ascribed to the C═O stretching vibrational spectrum. With respect to the ones after UiO-66-NH_2 functionalization, many obvious absorption peaks appeared. They are obviously different from the features of CF-COOH, which is attributed to that external MOF coating covered up the pristine carboxylated surfaces of CF-COOH. For instance, the broad and intense spectrum ranged from 3580 to 3000 cm^{-1} is ascribed to the synergistic effects between stretching vibration of −OH groups and symmetric and asymmetric stretching vibration of $-NH_2$ groups. The isolated peak at 1658 cm^{-1} is attributed to the deformation vibration $\delta(NH_2)$ of $-NH_2$ groups, while the typical 1606−1485 cm^{-1} interval bands due to the aromatic C−C ring vibration modes are visible. Moreover, a component located at 1400 cm^{-1} corresponds to the OCO symmetric stretching, and 1257 cm^{-1} assigned to the C−N stretching vibrational spectrum. The Zr-(OC) symmetric and asymmetric stretchings are characterized by 622 and 560 cm^{-1}, respectively. The FTIR spectra confirm the successful MOF "armor" covering on the fiber surface compared with the feature peaks detected from its homogeneous nucleated product.

The surface chemistry of various CFs without and with a MOF "armor" was studied by X-ray photoelectron spectroscopy (XPS) (Figure 3). The UiO-66-NH_2-grown CFs are denoted as CF-UiO-66-NH_2 and are appended with "-*n* h" according to the detailed incubation (crystallization) time of *n* hours. From the wide spectra (Figure 3A), CF-UiO-66-NH_2 shows a typical Zr 3d peak with a detailed devolution analysis in Figure 3B, which is clearly absent from pristine CFs and CF-COOH. Furthermore, the O composition and O/C atom ratio of CF-COOH and CF-UiO-66-NH_2 increase, and the O═C−O contents increase obviously (Figure 3C,D and Supporting Information, Table S1). The carboxyl groups can readily facilitate the heterogeneous crystallization of UiO-66-NH_2 onto the CF-COOH surface to form a homogeneous MOF coating (as shown in following SEM images) due to the template-induced nucleation of metal salt clusters on the acidized surface of 1D CFs via metal−carboxyl bonds, which is similar to the MOF growth on the mercaptohexadecanoic acid monolayer on the Au (111) surface.[49] CF-UiO-66-NH_2-36 h shows a C−N peak located at 285.8 eV and a Zr 3d fitting peak conforming to the results reported in the literature,[50] indicating the successful

DOI: 10.1021/acsami.6b15098
ACS Appl. Mater. Interfaces 2017, 9, 5590−5599

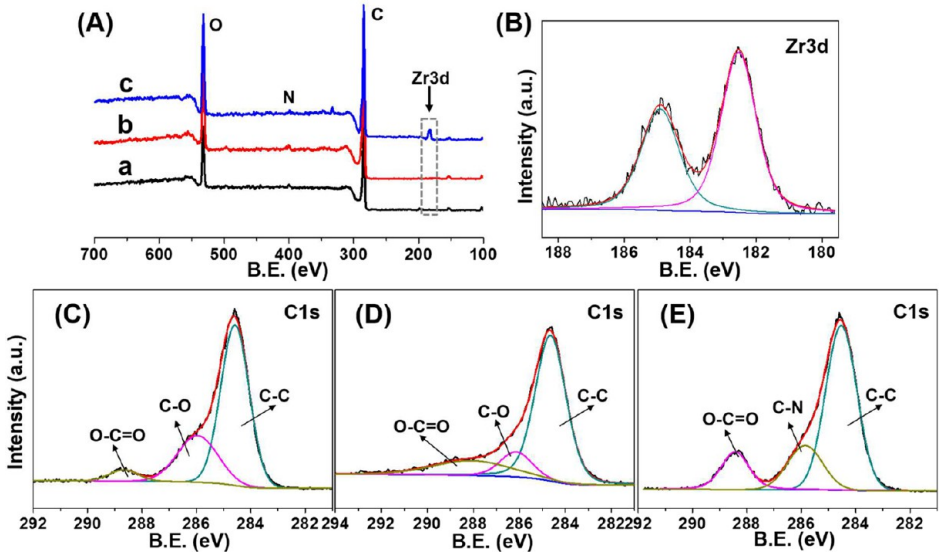

Figure 3. XPS analysis. (A) Wide-scan XPS spectra of (a) pristine CF, (b) acid-treated CF, and (c) CF-UiO-66-NH_2. XPS curve fitting for (B) Zr 3d peak of CF-UiO-66-NH_2, the C 1s spectra of (C) pristine CF, (D) CF-COOH, and (E) CF-UiO-66-NH_2.

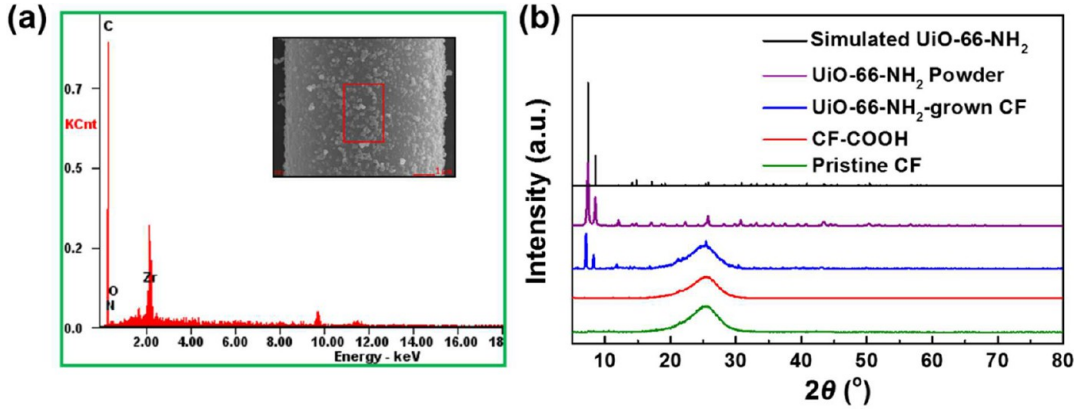

Figure 4. (a) EDX spectrum on a UiO-66-NH_2-grown CF. (b) XRD patterns of pristine CF, CF-COOH, UiO-66-NH_2-grown CF, UiO-66-NH_2 powder, and simulated UiO-66-NH_2.

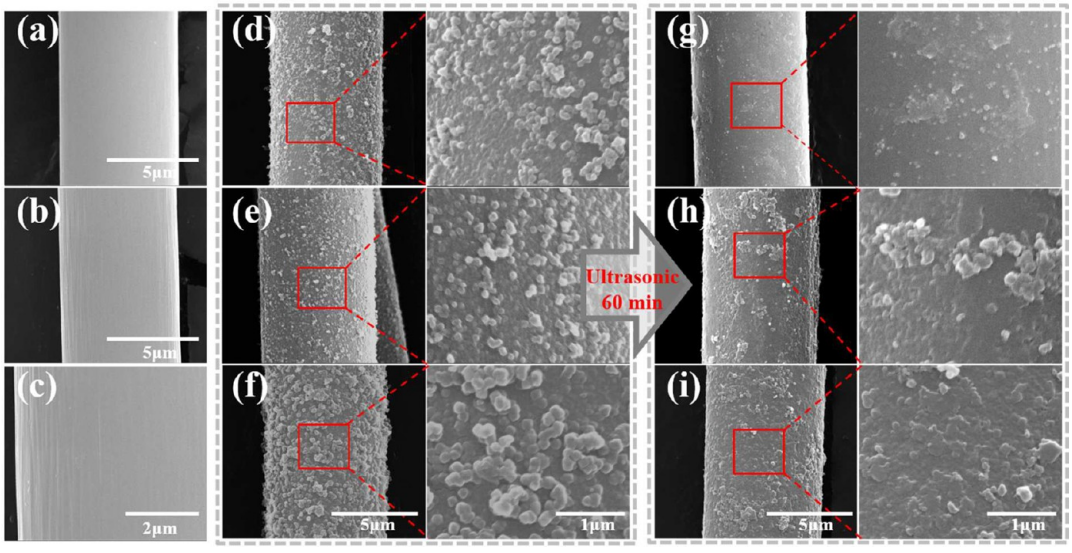

Figure 5. SEM images of (a) the pristine, (b, c) acid-treated CFs, (d, e, f) UiO-66-NH_2-functionalized fibers for 24, 36, and 48 h, and (g, h, i) corresponding fibers after ultrasonic treatment for 60 min.

DOI: 10.1021/acsami.6b15098
ACS Appl. Mater. Interfaces 2017, 9, 5590−5599

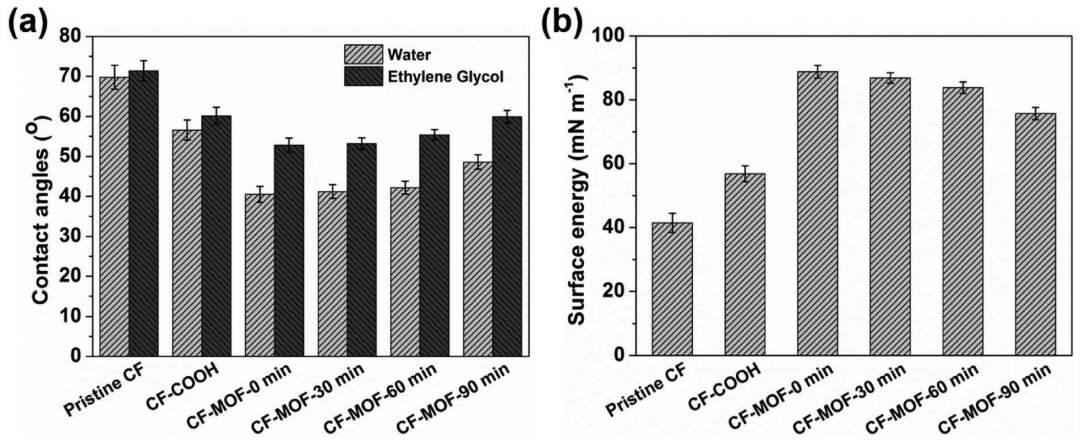

Figure 6. (a) Water and ethylene glycol contact angles and (b) resultant surface energy of various CFs, including pristine CF, CF-COOH, CF-MOF-0 min, CF-MOF-30 min, CF-MOF-30 min, and CF-MOF-90 min (MOF-*n* min denotes UiO-66-NH_2-36 h with *n* min sonication).

in situ growth of 3D MOF onto the 1D fiber surface (Figure 3B,E). Energy-dispersive X-ray (EDX) analysis also reveals distinct Zr atoms from the MOF coating (Figure 4a). The X-ray diffraction (XRD) patterns in Figure 4b exhibit several characteristic sharp peaks, consistent with the simulated UiO-66-NH_2 features. The broad composition located at $2\theta = 25.5°$ represents the typical turbostratic graphitic stacking structure of the carbon fibers.[51] The appearance of several new and prominent peaks on the UiO-66-NH_2 grown CFs which are absent in pristine CFs indicates the construction of a 3D MOF crystalline structure on the surface of the 1D CFs.

Scanning electron microscopy (SEM) was used to monitor the status of MOF growth (Figure 5). Axial grooves are visible on the acidized CFs (CF-COOH) compared to the smooth pristine CFs (Figure 5a–c and Figure S2). A uniform and dense MOF coating was achieved on the CFs after carboxylation compared to the chaotic coatings achieved without carboxylation (Figure S3). After incubation in the precursor mixture for 24, 36, or 48 h, the surface topographies of the CFs became rugged and adhered many surface-bound nanocrystals because of the physicochemical interactions of the surface-coated MOF with the nanocrystals and the high specific surface area of nanoporous UiO-66-NH_2 (Figure 5d–f).[39] Combined with the preliminary assay, ultrasonic treatment of the MOF-grown CFs was an effective way to remove the nanocrystals and was beneficial to the interfacial performance of the fiber-reinforced composites. When exposed to ultrasound, the CFs' surfaces became smoother, and the microscopic morphology was more flakelike than the previous ridge-and-valley of the surficial hierarchical structure (Figure 5g–i and Figures S4 and S5). Therefore, the attached nanocrystals can be gradually removed, and the "vulnerable" bonds between the MOF "armor" and the attached nanocrystals are broken with increasing the ultrasonic treatment time. Furthermore, the inner unsaturated dangling bonds on the CFs can lead to perfect crystallization with a longer incubation time, which improves the coating's resistance to ultrasound. Moreover, thermogravimetric analysis (TGA) measurements were also conducted on the CFs before and after the MOF "armor" coating under the same calcination procedure (Figure S6). The ~2 wt % weight loss difference between the pristine CFs and CF-UiO-66-NH_2-36 h up to more than 950 °C treatment indicates the formation of a good coating layer of MOF on the 1D CF surface, and the similar curve tendency indicates excellent thermal stability of the MOF-grown CFs.

The surface energy of fibers is crucial for fiber-reinforced composites because it governs the resin impregnation onto the fibers.[19,52,53] The surface energy is typically determined as a sum of the dispersive and polar components of fibers and can be statistically calculated using the water and ethylene glycol contact angles according to eqs 1 and 2:

$$\gamma_l(1 + \cos\theta) = 2(\gamma_l^p\gamma_f^p)^{1/2} + 2(\gamma_l^d\gamma_f^d)^{1/2} \quad (1)$$

$$\gamma_f = \gamma_f^d + \gamma_f^p \quad (2)$$

where γ represents the surface energy, the subscripts l and f stand for immersion liquid and fiber, and the superscripts d and p stand for dispersive and polar components, respectively. θ refers to the corresponding contact angles. To investigate the effects of the MOF coating and ultrasound treatment time on the surface energy, the CF-UiO-66-NH_2-36 h samples were treated with ultrasound for varying amounts of time from 0 to 90 min (the samples are denoted by CF-MOF-0 min, CF-MOF-30 min, CF-MOF-60 min, and CF-MOF-90 min). From Figure 6 and Table S2, an increase of surface energy is apparent on MOF-grown CFs compared to that of pristine CFs or CF-COOH. Compared to the surface energy value of the pristine fibers (41.47 mN m^{-1}), the surface energy increment of CF-MOF-0 min (without ultrasound) and CF-MOF-60 min (with ultrasound) is 114% and 102%, respectively. The polar functional groups and nanoporous organic–inorganic hybrid structure of the MOF "armor" and the attached nanocrystals significantly increase the polar compositions of the integral surface energy. Further sonication processing had a slight negative effect on the detailed values due to the "cleaning" effect of the ultrasonic treatment. Although a shorter sonication time results in more nanocrystals attached to the surface and the subsequently larger roughness, which is beneficial for the surface energy, a longer sonication time (60 min) is preferred to completely remove the nanocrystals from the 1D fibers (Figure 5) and to eliminate the possible "weak" surface/interface points in the composites after template-induced nucleation of MOF, as shown in the following discussions on the fiber strength and composite mechanical properties. To better illustrate the contribution of UiO-66-NH_2 coating to enhance the compatibility between CF and epoxy resin, the surface energy of epoxy resin was measured. As a result, the

DOI: 10.1021/acsami.6b15098
ACS Appl. Mater. Interfaces 2017, 9, 5590–5599

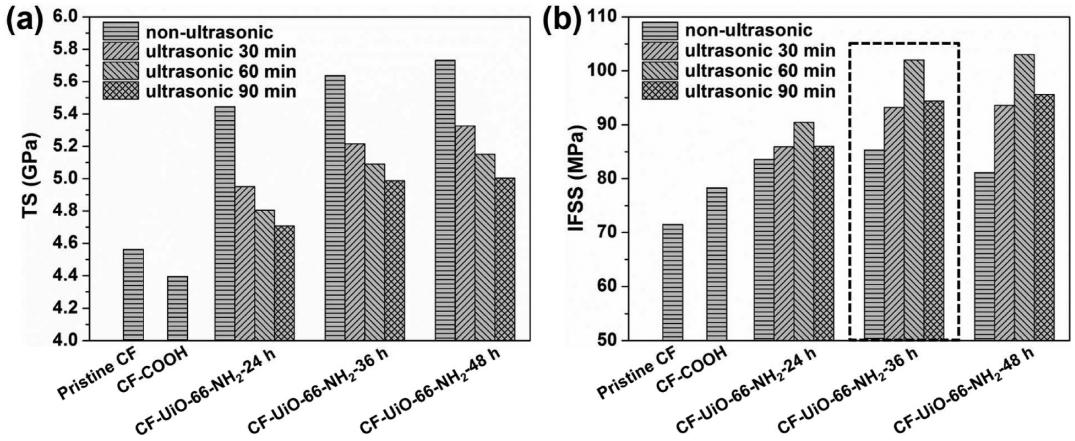

Figure 7. (a) TS of various fiber filaments, including pristine CF, CF-COOH, UiO-66-NH_2-24, -36, and -48 h and (b) IFSS of the corresponding CF/epoxy matrix composites.

surface energy of epoxy resin is 55.1 mN m^{-1}. The surface energy value of the pristine fibers is below that of epoxy resin. Thus, the epoxy resin could not effectively impregnate the pristine CFs. The surface energy of CF-MOF (Table S2) is beyond 75 mN m^{-1}; it is a relatively high energy surface as compared to the aforementioned two surface energies. Thus, the elevated surface energy of modified fibers can effectively facilitate the resin impregnation onto the surfaces.

3.2. Mechanical Property Measurements of CFs and Composites. The corresponding parameters, such as TS and IFSS, are significant to evaluate the overall mechanical properties of the modified CFs and relevant composites (Figure 7). TS is an inherent mechanical property of fibers and can be characterized by single-filament tensile testing. The TS of fibers affects the in-plane properties of the resulting composites.[1,18,19] As mentioned above, the traditional surface modification on fibers generally damages the surface structure, which has a negative effect on the TS of the fibers.[19,24−30] Therefore, it is extremely challenging to improve the TS of CFs using only surface modification approaches. Herein, we tested the tensile strengths of various CFs without or with the MOF "armor". All data are statistically analyzed using the Weibull distribution function in consideration of the high scattered trait of CFs.[1,54] The relevant thicknesses of MOF layer grown on CFs are listed in Table S3. As shown in Figure 7a, CF-COOH showed a slight decrease in TS (4.40 GPa) compared to that (4.56 GPa) of the pristine CFs because the etching of the superficial graphitic basal planes causes defects and striations.[21,55] Surprisingly, the TS of the MOF-grown CFs showed an increase compared with the pristine CFs or CF-COOH. This unexpected result indicates that the integral MOF "armor" constructed by template-induced nucleation on the surface of fibers improved the in-plane properties of the CFs. As shown in Figure 8, Zr−oxo clusters can be anchored on the active sites (−COOH groups) scattered on the surfaces of acid-treated CFs, based on which the well-defined scaffolded UiO-66-NH_2 frameworks can be constructed via constant supply of Zr^{4+} ions and NH_2-H_2BDC ligands in the precursor solution. The scheme exhibits a possible repair mechanism toward the axial grooves on the acid-treated CFs by utilizing its superficial −COOH groups to construct an intergrown MOF "armor". The Weibull shape parameter of various CFs did not vary noticeably, demonstrating a similar scatter degree of the fiber TS (Table S4). Without ultrasonic treatment, the TS increment

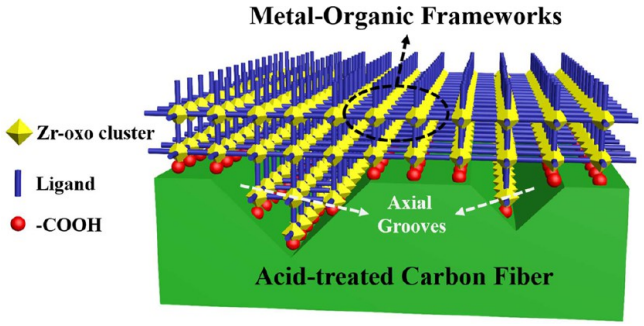

Figure 8. Schematic illustration of the possible repair mechanism toward the axial grooves on the acid-treated CFs by utilizing its exterior −COOH groups to construct UiO-66-NH_2 frameworks.

of CFs is much larger. The amplification of the TS of CFs after a 36 h incubation is generally greater than 10% compared with pristine CFs. The TSs of the remnant CFs showed a gradual decrease with increased the ultrasonic treatment time. In fact, the MOF coating is just like an "armor" on the CF surface, combining chemical and nonchemical bond interactions between $-NH_2$, −COOH, and Zr^{4+} through a synergistic effect. After applying a slight exterior tension, the defective positions on the surfaces of the applied CFs develop into cracks. During the spreading process, the cracks encounter the 3D MOF "armor" and the propagation direction detours, which can generate more tiny cracks and consume more damage energy. The MOF "armor" can withstand flaw expansion and protect CFs from being pulled apart. Therefore, MOF-grown fibers can effectively absorb more external stress and lessen the damage impact compared with pristine CFs.

The mechanical strength of fiber-reinforced composites is extremely important. Typically, IFSS is a simple way to predict the ideal mechanical properties of fiber-reinforced composites, which is determined through single-filament pull-out tests and is calculated using eq 3:

$$\mathrm{IFSS} = \frac{F_{\max}}{\pi d l} \tag{3}$$

where F_{max} is the maximum load displayed, d is the single-filament diameter, and l is the embedded length of a resin droplet. According to Figure 7b, our pristine CF has an IFSS of 71.5 MPa. The IFSS of CF-COOH is slightly higher than that of pristine CFs due to the larger polar compositions and

DOI: 10.1021/acsami.6b15098
ACS Appl. Mater. Interfaces 2017, 9, 5590−5599

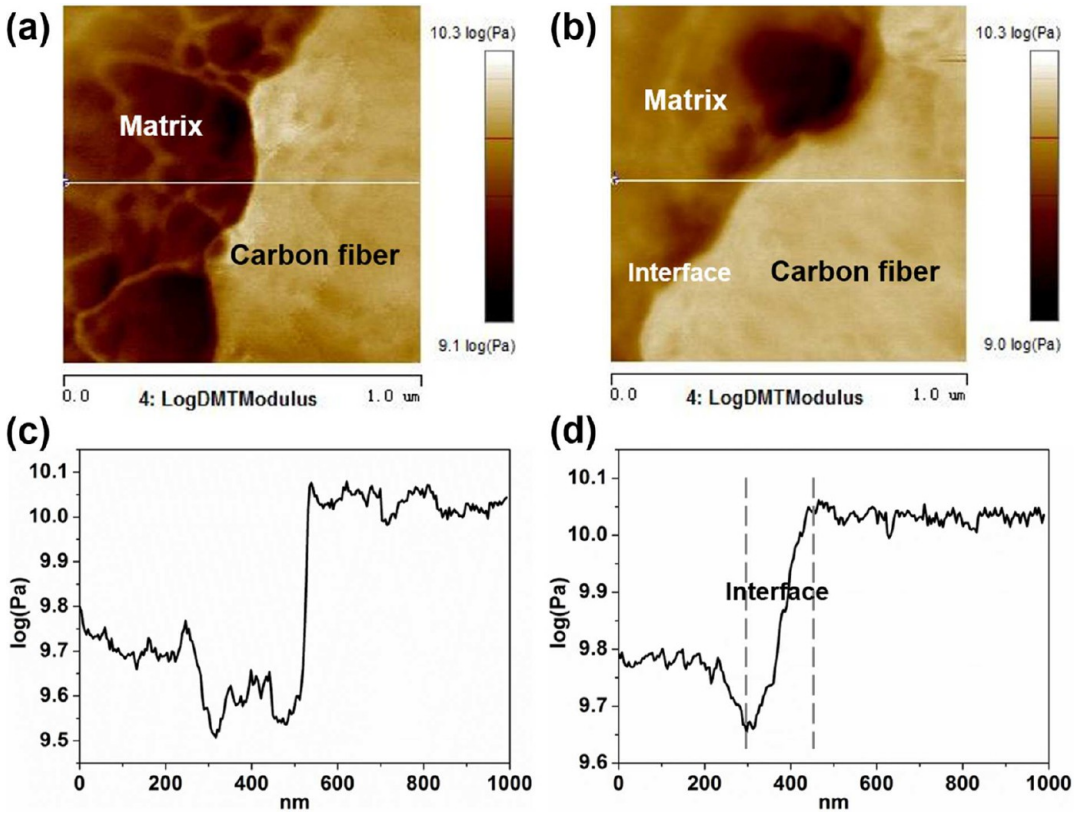

Figure 9. AFM force modulation images and section analysis of the interphase in composites enhanced by (a, c) the pristine CFs and (b, d) CF-UiO-66-NH_2-36 h.

longitudinal grooves for mechanical interlocking. For UiO-66-NH_2 grown CFs, even after washing several times, there are still nanocrystals on the fiber surfaces (Figure 5d–f). When cured with epoxy resin, the amino groups hanging outside at the linker units of the UiO-66-NH_2 coatings, as well as the exterior nanocrystals, react with the epoxy groups, which can contribute to strong adhesion between the CFs and epoxy matrix. The interactions (van der Waals attraction and hydrogen bonds between $-NH_2$, $-COOH$, and Zr^{4+}) between the MOF coating and the nanocrystals are generally fragile under external factors, such as ultrasonic treatment and slight force, when compared to Zr–O coordination bonds. The "vulnerable" bonds between the MOF "armor" and the attached nanocrystals provide a lubricant effect with respect to the areas covered by the "firm" bonds between MOF and the fibers. Therefore, without ultrasonic treatment, the IFSS value of the composite formed by MOF-grown CFs only demonstrates a slight enhancement.[56,57] Based on the histogram, without ultrasonic treatment, the IFSS value of CF-UiO-66-NH_2-48 h tends to decrease compared with that of the 36 h sample. This decrease is attributed to the more serious aggregation of surface-attached nanocrystals (Figure 5e,f). Ultrasonic treatment of the MOF-grown CFs is very efficient for reducing the "lubricant" effect and maintaining the "fortified" effect. After a certain amount of ultrasonic exposure of the MOF-grown CFs, the negative lubricating effect is almost eliminated. A uniform, flakelike morphology of the MOF coating is achieved along with a corresponding enhancement of the mechanical properties due to the closer interactions between the resin and MOF "armor" and results in the formation of a stable intermediate zone. For ultrasonic treatment of MOF-grown CFs for different times (0, 30, 60, and 90 min), the IFSS values show a gradient enhancement initially (within 60 min) and then decline (beyond 60 min). The samples with 60 min ultrasonic treatment have the highest IFSS value and balanced flexibility. Furthermore, the IFSS value after excessive ultrasonic treatment (90 min) decreases due to the out-of-balance status between the chemical and nonchemical bonds induced by excessive ultrasonic cavitation.[56,57] Marked by the interrupted black frame, CF-UiO-66-NH_2-36 h, with 60 min ultrasonic treatment, has an IFSS value of 103 MPa, which is 44.1% higher than that (71.5 MPa) of the pristine CFs. This difference is attributed to the reaction between the amino groups on the outside of the linker units of the UiO-66-NH_2 coating and epoxy resin, which strongly fortify the fiber/resin interface, and the extremely stable structure of UiO-66 type MOF arising from the large coordination number of 12.[36] Such high IFSS values of the composite MOF "armor" grown CFs (exceeding 100 MPa) are seldom reported in the literature (Table S5).

For further exploration of the fiber/resin interfacial status and mechanical properties of CF-reinforced composites for "real-world" applications, the interfacial modulus, interlaminar shear strength, and cross-sectional views of fractured regions were characterized. The interfacial modulus evaluation was implemented using AFM in the force modulation mode. The generated images were produced in accordance with the fluctuating response of the test tip under scanning. As shown in Figure 9, an obvious difference between the composites fabricated by CFs without and with the MOF "armor" is clearly observed in the middle of the two phases. For the pristine CF-enhanced composites (Figure 9a,c), two separate phases were displayed, and the modulus curve varied sharply

DOI: 10.1021/acsami.6b15098
ACS Appl. Mater. Interfaces 2017, 9, 5590–5599

from the left matrix region to the right fiber region, indicated by the white line. The remarkable variation of the modulus on the two-phase boundary is related to the nonideal chemical interactions on the inert carbon fiber skin. In contrast, the MOF "armor"-grown CF-reinforced composite shows a clear gradient transition on the modulus with an intermediate gradient region between the fiber and the matrix regions (Figure 9b,d). The elevated polar surface energy and enriched polar groups stimulate the reactivity between the matrix and the MOF coating on the CFs, which accelerates the curing process of the CFs and epoxy resin. These unique merits of the interphase enable it to act as a "cushion" in the process of exterior stress transfer and improve the load implementation efficiency.

The ILSS reflects the overall mechanical features of the overall composite material reinforced with CFs for practical applications. The ILSS is calculated using eq 4:

$$\mathrm{ILSS} = \frac{3P_b}{4bh} \tag{4}$$

where P_b is the maximum load recorded during the fracture measurement, b is the width of the testing composites, and h is the thickness. Referring to Figure 10, the ILSS varied slightly

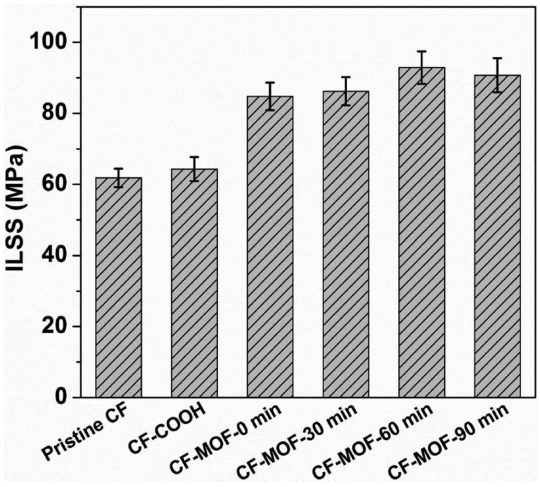

Figure 10. Interlaminar shear strength (ILSS) measurement of the composites composed of the pristine CFs, CF-MOF-x min (sonication for 0, 30, 60, and 90 min) with UiO-66-NH_2 grown for 36 h.

from the pristine CF-fabricated composites (61.83 MPa) to the CF-COOH composites (64.29 MPa). Based on the histogram, the increasing percentages of the ILSS values of the MOF-grown CF-reinforced composites compared to the pristine CF-reinforced composites are generally greater than 37%. Sonication can remove the attached microcrystals (as shown in Figure 5) to optimize the amount of exposed surface of the MOF "armor" toward the resin, contributing to greater compatibility of the two disparate substances. As a result, ILSS can reach 92.88 MPa, which is a 50.2% increase compared to the pristine material under the optimal conditions. This value is among the highest values of ILSS reported in the literature (Table S6).

The cross-sectional fractured regions were examined by SEM to analyze the interface adhesion status and the microcracks generating mechanism behind the outer impact on the inner composites from the crack tips caused by the previous ILSS test experiments. The results are shown in Figure 11 and Figure S7.

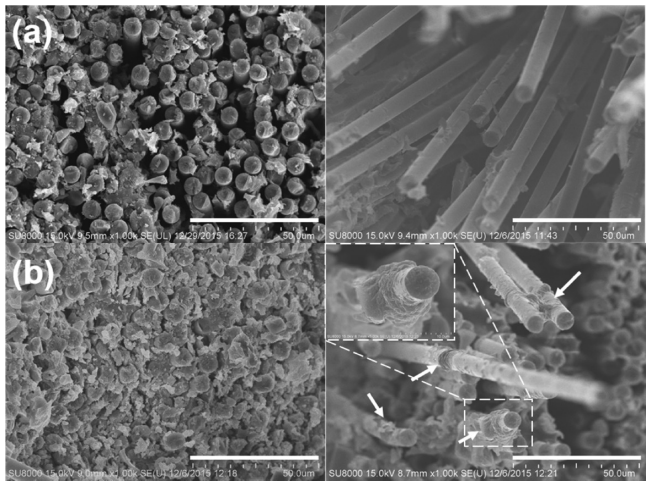

Figure 11. SEM images of the fractured composites made with (a) the pristine CFs and (b) CF-UiO-66-NH_2-36 h with sonication for 60 min (scale bar: 50 μm). The white arrows point to the resin affixed on the protuberant CFs in the marginal region (right-sided SEM images), and the inset image is a high magnification of a typical region.

As Figure 11a shows, a loose combination and obvious segregation between the fibers and epoxy matrix in the presence of many nearly glabrous fibers detached from the matrix resin can be observed in the pristine CF-reinforced composites. The pristine CFs initially bury and accelerate certain potential defects and hazards that facilitate the crack evolution in the front of the impact loading in the progress of composite fabrication. Beneath the superficial phenomena, the following factors play a crucial role on a theoretical level: the sleek fiber skins, the poor wettability, and the nonideal chemical interactions due to the negligible polar group density.[11−13] For the sample derived from the MOF "armor"-grown CFs, several small chippings adhered to the cracked regions. Because of the multifunctional effects of the MOF "armor" on the fiber strength and composite strength, there is a well-adhered status between the MOF-grown CFs and the matrix resin (Figure 11b). A typical margin region and its magnification view (the inset image) show the detailed horizon of the filament and matrix adhesion, and the white arrows indicate the residual resin immobilized on the fractured CFs. The tightly adherent resin on the CFs grown with MOF indicates highly anomalous cracked topography, confirming the occurrence of favorable interfacial chemical bonding reactions. The inner interface can induce dendritic cracks from the force bearing point, resulting in a subsequent similar trend of crack propagation from the newly generated sites. The "eye-guided" cross-sectional SEM images of the fractured samples provide vivid proof of the excellent interface between the fibers and polymer matrix due to the template-induced growth of the MOF "armor" on the fibers.

4. CONCLUSIONS

In situ growth of a 3D MOF dense "armor" on the surface of 1D fibers was reported by template-induced nucleation. Taking advantage of MOF as a novel interfacial linker between the fiber and polymer matrix and a smart cushion to release interior and exterior applied forces, an unusual simultaneous enhancement of the interfacial and interlaminar shear strength, as well as the tensile strength, of CFs can be achieved. With the aid of an ultrasonic "cleaning" process, the optimized surface energy and

DOI: 10.1021/acsami.6b15098
ACS Appl. Mater. Interfaces 2017, 9, 5590−5599

tensile strength of CFs with a 3D MOF "armor" are 83.79 mN m^{-1} and 5.09 GPa, which is an increase of 102% and 11.6%, respectively. The IFSS and ILSS of the resultant composites reach as high as 103 and 92.88 MPa, respectively. Our work suggests that the template-induced nucleation of 3D MOF onto 1D fibers can be used as a general approach for advanced composite materials for diverse scientific and technical applications.

■ ASSOCIATED CONTENT

Supporting Information

The Supporting Information is available free of charge on the ACS Publications website at DOI: 10.1021/acsami.6b15098.

Optical images of the dynamic angle test machine and operational schematic illustration, SEM images of UiO-66-NH_2 grown CFs with/without carboxylation pretreatment, SEM and cross-sectional SEM images of UiO-66-NH_2-functionalized carbon fibers after ultrasonic exposure, TGA traces of pristine CF and CF-UiO-66-NH_2, SEM images of the fractured carbon fiber/epoxy composites, surface element characterization, surface energy evaluation, single fiber tensile strength of CFs, referenced IFSS and ILSS of CF/epoxy resin composites (PDF)

■ AUTHOR INFORMATION

Corresponding Authors

*E-mail: zguo10@utk.edu (Z.G.).
*E-mail: shaolu@hit.edu.cn, odysseynus@hotmail.com (L.S.).

ORCID

Zhanhu Guo: 0000-0003-0134-0210
Lu Shao: 0000-0002-4161-3861

Author Contributions

X.Y. and X.J. contributed equally.

Notes

The authors declare no competing financial interest.

■ ACKNOWLEDGMENTS

This work was financially supported by National Natural Science Foundation of China (21676063, U1462103), Harbin Science and Technology Innovation Talent Funds (2014RFXXJ028), and HIT Environment and Ecology Innovation Special Funds (HSCJ201619). Dr. Z. Guo specially appreciates the ACS PRF supports.

■ REFERENCES

(1) Paiva, M. C.; Bernardo, C. A.; Nardin, M. Mechanical, Surface and Interfacial Characterisation of Pitch and PAN-based Carbon Fibres. *Carbon* **2000**, *38*, 1323−1337.

(2) Chung, D. D. L. *Carbon Fiber Composites*; Butterworth-Heinemann: 2012.

(3) Mukherjee, M.; Das, C. K.; Kharitonov, A. P.; Banik, K.; Mennig, G.; Chung, T. N. Properties of Syndiotactic Polystyrene Composites with Surface Modified Short Kevlar Fiber. *Mater. Sci. Eng., A* **2006**, *441*, 206−214.

(4) Xu, Z.; Gao, C. Graphene Fiber: A New Trend in Carbon Fibers. *Mater. Today* **2015**, *18*, 480−492.

(5) Zhang, J.; Feng, W.; Zhang, H.; Wang, Z.; Calcaterra, H. A.; Yeom, B.; Hu, P. A.; Kotov, N. A. Multiscale Deformations Lead to High Toughness and Circularly Polarized Emission in Helical Nacre-like Fibres. *Nat. Commun.* **2016**, *7*, 10701.

(6) Gao, S. L.; Mäder, E.; Zhandarov, S. F. Carbon Fibers and Composites with Epoxy Resins: Topography, Fractography and Interphases. *Carbon* **2004**, *42*, 515−529.

(7) Tran, M. Q.; Ho, K. K.; Kalinka, G.; Shaffer, M. S.; Bismarck, A. Carbon Fibre Reinforced Poly (Vinylidene Fluoride): Impact of Matrix Modification on Fibre/Polymer Adhesion. *Compos. Sci. Technol.* **2008**, *68*, 1766−1776.

(8) Kuttner, C.; Tebbe, M.; Schlaad, H.; Burgert, I.; Fery, A. Photochemical Synthesis of Polymeric Fiber Coatings and Their Embedding in Matrix Material: Morphology and Nanomechanical Properties at the Fiber-Matrix Interface. *ACS Appl. Mater. Interfaces* **2012**, *4*, 3484−3492.

(9) Chen, S.; Cao, Y.; Feng, J. Polydopamine as An Efficient and Robust Platform to Functionalize Carbon Fiber for High-Performance Polymer Composites. *ACS Appl. Mater. Interfaces* **2013**, *6*, 349−356.

(10) Gu, H.; Guo, J.; Wei, H.; Guo, S.; Liu, J.; Huang, Y.; Khan, M. A.; Wang, X.; Young, D. P.; Wei, S.; Guo, Z. Strengthened Magnetoresistive Epoxy Nanocomposite Papers Derived from Synergistic Nanomagnetite-Carbon Nanofiber Nanohybrids. *Adv. Mater.* **2015**, *27*, 6277−6282.

(11) Hamerton, I.; Hay, J. N.; Howlin, B. J.; Jones, J. R.; Lu, S. Y. Molecular Modelling of Interactions at the Composite Interface between Surface-Treated Carbon Fibre and Polymer Matrices: The Influence of Surface Functional Groups. *J. Mater. Chem.* **1998**, *8*, 1333−1337.

(12) Montes-Moran, M. A.; Young, R. J. Raman Spectroscopy Study of HM Carbon Fibres: Effect of Plasma Treatment on the Interfacial Properties of Single Fibre/Epoxy Composites. *Carbon* **2002**, *40*, 845−855.

(13) Pamula, E.; Rouxhet, P. G. Bulk and Surface Chemical Functionalities of Type III PAN-based Carbon Fibres. *Carbon* **2003**, *41*, 1905−1915.

(14) Jiang, D.; Liu, L.; Long, J.; Xing, L.; Huang, Y.; Wu, Z.; Yan, X.; Guo, Z. Reinforced Unsaturated Polyester Composites by Chemically Grafting Amino-POSS onto Carbon Fibers with Active Double Spiral Structural Spiralphosphodicholor. *Compos. Sci. Technol.* **2014**, *100*, 158−165.

(15) Cao, H.; Huang, Y.; Zhang, Z.; Sun, J. Uniform Modification of Carbon Fibers Surface in 3-D Fabrics Using Intermittent Electrochemical Treatment. *Compos. Sci. Technol.* **2005**, *65*, 1655−1662.

(16) Morán, M. M.; Van Hattum, F. W. J.; Nunes, J. P.; Martínez, A. A.; Tascón, J. M. D.; Bernardo, C. A. A Study of the Effect of Plasma Treatment on the Interfacial Properties of Carbon Fibre-Thermoplastic Composites. *Carbon* **2005**, *43*, 1795−1799.

(17) Xu, Z.; Huang, Y.; Zhang, C.; Liu, L.; Zhang, Y.; Wang, L. Effect of γ-Ray Irradiation Grafting on the Carbon Fibers and Interfacial Adhesion of Epoxy Composites. *Compos. Sci. Technol.* **2007**, *67*, 3261−3270.

(18) Lin, Y.; Ehlert, G.; Sodano, H. A. Increased Interface Strength in Carbon Fiber Composites through a ZnO Nanowire Interphase. *Adv. Funct. Mater.* **2009**, *19*, 2654−2660.

(19) Zhao, F.; Huang, Y. Preparation and Properties of Polyhedral Oligomeric Silsesquioxane and Carbon Nanotube Grafted Carbon Fiber Hierarchical Reinforcing Structure. *J. Mater. Chem.* **2011**, *21*, 2867−2870.

(20) Zhao, F.; Huang, Y. Grafting of Polyhedral Oligomeric Silsesquioxanes on a Carbon Fiber Surface: Novel Coupling Agents for Fiber/Polymer Matrix Composites. *J. Mater. Chem.* **2011**, *21*, 3695−3703.

(21) Peng, Q.; He, X.; Li, Y.; Wang, C.; Wang, R.; Hu, P.; Yan, Y.; Sritharan, T. Chemically and Uniformly Grafting Carbon Nanotubes onto Carbon Fibers by Poly (Amidoamine) for Enhancing Interfacial Strength in Carbon Fiber Composites. *J. Mater. Chem.* **2012**, *22*, 5928−5931.

(22) Guo, W.; Zhang, F.; Lin, C.; Wang, Z. L. Direct Growth of TiO_2 Nanosheet Arrays on Carbon Fibers for Highly Efficient Photocatalytic Degradation of Methyl Orange. *Adv. Mater.* **2012**, *24*, 4761−4764.

(23) Zhang, L.; Ding, Q.; Huang, Y.; Gu, H.; Miao, Y. E.; Liu, T. Flexible Hybrid Membranes with $Ni(OH)_2$ Nanoplatelets Vertically

Grown on Electrospun Carbon Nanofibers for High-Performance Supercapacitors. *ACS Appl. Mater. Interfaces* **2015**, *7*, 22669−22677.
(24) Down, W. B.; Baker, R. T. K. Modification of the Surface Properties of Carbon Fibers via the Catalytic Growth of Carbon Nanofibers. *J. Mater. Res.* **1995**, *10*, 625−633.
(25) Thostenson, E. T.; Li, W. Z.; Wang, D. Z.; Ren, Z. F.; Chou, T. W. Carbon Nanotube/Carbon Fiber Hybrid Multiscale Composites. *J. Appl. Phys.* **2002**, *91*, 6034−6037.
(26) Zhao, Z. G.; Ci, L. J.; Cheng, H. M.; Bai, J. B. The Growth of Multi-Walled Carbon Nanotubes with Different Morphologies on Carbon Fibers. *Carbon* **2005**, *43*, 663−665.
(27) Xie, J.; Xin, D.; Cao, H.; Wang, C.; Zhao, Y.; Yao, L.; Ji, F.; Qiu, Y. Improving Carbon Fiber Adhesion to Polyimide with Atmospheric Pressure Plasma Treatment. *Surf. Coat. Technol.* **2011**, *206*, 191−201.
(28) Zhang, X.; Fan, X.; Yan, C.; Li, H.; Zhu, Y.; Li, X.; Yu, L. Interfacial Microstructure and Properties of Carbon Fiber Composites Modified with Graphene Oxide. *ACS Appl. Mater. Interfaces* **2012**, *4*, 1543−1552.
(29) Qian, H.; Bismarck, A.; Greenhalgh, E. S.; Kalinka, G.; Shaffer, M. S. Hierarchical Composites Reinforced with Carbon Nanotube Grafted Fibers: The Potential Assessed at the Single Fiber Level. *Chem. Mater.* **2008**, *20*, 1862−1869.
(30) Zhao, F.; Huang, Y. Uniform Modification of Carbon Fibers in High Density Fabric by γ-Ray Irradiation Grafting. *Mater. Lett.* **2011**, *65*, 3351−3353.
(31) Jiang, J.; Yaghi, O. M. Brønsted Acidity in Metal-Organic Frameworks. *Chem. Rev.* **2015**, *115*, 6966−6997.
(32) Valenzano, L.; Civalleri, B.; Chavan, S.; Bordiga, S.; Nilsen, M. H.; Jakobsen, S.; Lillerud, K. P.; Lamberti, C. Disclosing the Complex Structure of UiO-66 Metal Organic Framework: A Synergic Combination of Experiment and Theory. *Chem. Mater.* **2011**, *23*, 1700−1718.
(33) Zhang, W.; Liu, Y.; Lu, G.; Wang, Y.; Li, S.; Cui, C.; Wu, J.; Xu, Z.; Tian, D.; Huang, W.; DuCheneu, J. S.; et al. Mesoporous Metal-Organic Frameworks with Size-, Shape-, and Space-Distribution-Controlled Pore Structure. *Adv. Mater.* **2015**, *27*, 2923−2929.
(34) Li, H.; Sadiq, M. M.; Suzuki, K.; Ricco, R.; Doblin, C.; Hill, A. J.; Lim, S.; Falcaro, P.; Hill, M. R. Magnetic Metal-Organic Frameworks for Efficient Carbon Dioxide Capture and Remote Trigger Release. *Adv. Mater.* **2016**, *28*, 1839−1844.
(35) Zhai, Q. G.; Bu, X.; Mao, C.; Zhao, X.; Feng, P. Systematic and Dramatic Tuning on Gas Sorption Performance in Heterometallic Metal-Organic Frameworks. *J. Am. Chem. Soc.* **2016**, *138*, 2524−2527.
(36) Cavka, J. H.; Jakobsen, S.; Olsbye, U.; Guillou, N.; Lamberti, C.; Bordiga, S.; Lillerud, K. P. A New Zirconium Inorganic Building Brick Forming Metal Organic Frameworks with Exceptional Stability. *J. Am. Chem. Soc.* **2008**, *130*, 13850−13851.
(37) Vermoortele, F.; Ameloot, R.; Vimont, A.; Serre, C.; De Vos, D. An Amino-Modified Zr-terephthalate Metal-Organic Framework as An Acid-Base Catalyst for Cross-Aldol Condensation. *Chem. Commun.* **2011**, *47*, 1521−1523.
(38) Nik, O. G.; Chen, X. Y.; Kaliaguine, S. Functionalized Metal Organic Framework-Polyimide Mixed Matrix Membranes for CO_2/CH4 Separation. *J. Membr. Sci.* **2012**, *413*, 48−61.
(39) Kandiah, M.; Nilsen, M. H.; Usseglio, S.; Jakobsen, S.; Olsbye, U.; Tilset, M.; Larabi, C.; Quadrelli, E. A.; Bonino, F.; Lillerud, K. P. Synthesis and Stability of Tagged UiO-66 Zr-MOFs. *Chem. Mater.* **2010**, *22*, 6632−6640.
(40) Nazari, M.; Rubio-Martinez, M.; Tobias, G.; Barrio, J. P.; Babarao, R.; Nazari, F.; Konstas, K.; Muir, B. W.; Collins, S. F.; Hill, A. J.; Duke, M. C.; Hill, M. R. Metal-Organic-Framework-Coated Optical Fibers as Light-Triggered Drug Delivery Vehicles. *Adv. Funct. Mater.* **2016**, *26*, 3244−3249.
(41) Wu, H.; Yildirim, T.; Zhou, W. Exceptional Mechanical Stability of Highly Porous Zirconium Metal−Organic Framework UiO-66 and its Important Implications. *J. Phys. Chem. Lett.* **2013**, *4*, 925−930.
(42) Musto, P.; Martuscelli, E.; Ragosta, G.; Mascia, L. Cure Kinetics and Ultimate Properties of a Tetrafunctional Epoxy Resin Toughened by a Perfluoro-Ether Oligomer. *Polymer* **2001**, *42*, 5189−5198.
(43) Jahan, M.; Bao, Q.; Yang, J. X.; Loh, K. P. Structure-Directing Role of Graphene in the Synthesis of Meta-Organic Framework Nanowire. *J. Am. Chem. Soc.* **2010**, *132*, 14487−14495.
(44) Hu, Y.; Wei, J.; Liang, Y.; Zhang, H.; Zhang, X.; Shen, W.; Wang, H. Zeolitic Imidazolate Framework/Graphene Oxide Hybrid Nanosheets as Seeds for the Growth of Ultrathin Molecular Sieving Membranes. *Angew. Chem., Int. Ed.* **2016**, *55*, 2048−2052.
(45) Yin, Y.; Alivisatos, A. P. Colloidal Nanocrystal Synthesis and the Organic−Inorganic Interface. *Nature* **2005**, *437*, 664−670.
(46) Liu, Y.; Goebl, J.; Yin, Y. Templated Synthesis of Nano-structured Materials. *Chem. Soc. Rev.* **2013**, *42*, 2610−2653.
(47) Wang, Y.; He, J.; Liu, C.; Chong, W. H.; Chen, H. Thermodynamics Versus Kinetics in Nanosynthesis. *Angew. Chem., Int. Ed.* **2015**, *54*, 2022−2051.
(48) Anjum, M. W.; Vermoortele, F.; Khan, A. L.; Bueken, B.; De Vos, D. E.; Vankelecom, I. F. Modulated UiO-66-Based Mixed-Matrix Membranes for CO_2 Separation. *ACS Appl. Mater. Interfaces* **2015**, *7*, 25193−25201.
(49) Scherb, C.; Schödel, A.; Bein, T. Directing the Structure of Metal-Organic Frameworks by Oriented Surface Growth on An Organic Monolayer. *Angew. Chem.* **2008**, *120*, 5861−5863.
(50) Long, J.; Wang, S.; Ding, Z.; Wang, S.; Zhou, Y.; Huang, L.; Wang, X. Amine-Functionalized Zirconium Metal-Organic Framework as Efficient Visible-Light Photocatalyst for Aerobic Organic Transformations. *Chem. Commun.* **2012**, *48*, 11656−11658.
(51) Huang, Y.; Young, R. J. Effect of Fibre Microstructure upon the Modulus of PAN-and Pitch-Based Carbon Fibres. *Carbon* **1995**, *33*, 97−107.
(52) Thornton, A. W.; Nairn, K. M.; Hill, J. M.; Hill, A. J.; Hill, M. R. Metal-Organic Frameworks Impregnated with Magnesium-Decorated Fullerenes for Methane and Hydrogen Storage. *J. Am. Chem. Soc.* **2009**, *131*, 10662−10669.
(53) Ma, L.; Meng, L.; Wang, Y.; Wu, G.; Fan, D.; Yu, J.; Qi, M.; Huang, Y. Interfacial Properties and Impact Toughness of Dendritic Hexamethylenetetramine Functionalized Carbon Fiber with Varying Chain Lengths. *RSC Adv.* **2014**, *4*, 39156−39166.
(54) Weibull, W.; Sweden, S. A Statistical Distribution Function of Wide Applicability. *J. Appl. Mech.* **1951**, *18*, 293−297.
(55) Pittman, C. U.; He, G. R.; Wu, B.; Gardner, S. D. Chemical Modification of Carbon Fiber Surfaces by Nitric Acid Oxidation Followed by Reaction with Tetraethylenepentamine. *Carbon* **1997**, *35*, 317−331.
(56) Huang, Y. D.; Liu, L.; Qiu, J. H.; Shao, L. Influence of Ultrasonic Treatment on the Characteristics of Epoxy Resin and the Interfacial Property of Its Carbon Fiber Composites. *Compos. Sci. Technol.* **2002**, *62*, 2153−2159.
(57) Lam, C. K.; Lau, K. T.; Cheung, H. Y.; Ling, H. Y. Effect of Ultrasound Sonication in Nanoclay Clusters of Nanoclay/Epoxy Composites. *Mater. Lett.* **2005**, *59*, 1369−1372.

DOI: 10.1021/acsami.6b15098
ACS Appl. Mater. Interfaces 2017, 9, 5590−5599